# Drivers of ecological success for *Escherichia coli* vary among human gut microbiome samples from different individuals

Mathilde Boumasmoud[1*], Ricardo León-Sampedro[1,2], Vera Beusch[1], Fabienne Benz[1,3] and Alex R. Hall[1]

1 Institute of Integrative Biology, Department of Environmental Systems Science, ETH Zurich, Zurich, Switzerland
2 Biomedical Research Networking Center for Epidemiology and Public Health (CIBERESP), Spain
3 Institut Pasteur, Université Paris Cité, CNRS UMR6047, Synthetic Biology, Paris 75015, France

*Corresponding author: mathilde.boumasmoud@env.ethz.ch

## Abstract

Gut microbial community composition varies from one person to another. Potentially, this means the ecological interactions experienced by individual strains or species also vary among microbiomes of different people. However, testing this directly in human microbiomes and identifying associated ecological drivers is challenging. Here, we use replicated anaerobic microcosms to quantify variability of population growth for a key commensal species among microbiome samples from different individuals, and to identify underlying intra- and interspecific interactions. In a reciprocal transplant experiment, both absolute and relative growth perfomance of different *Escherichia coli* strains varied among gut microbiome samples from different healthy individuals. This was partly explained by intraspecific competition: ecological success of individual *E. coli* strains was associated with displacement of resident conspecifics. However, the determinants of *E. coli* growth varied among samples from different individuals. In one microbiome sample with a distinctive taxonomic composition, culture acidification by resident microbes impaired growth of all *E. coli* strains. These results suggest inter-individual microbiome variation is a key driver of susceptibility to colonisation by incoming bacteria, impacting the relative success of different strains and thereby helping to explain the structure and diversity of human microbiomes.

## Introduction

Microbial colonization of the human gastrointestinal tract begins at birth [1]. After a dynamic development during the first years of life [2], microbial community composition remains relatively stable, with changes mostly in the relative abundances of different taxa [3]. Within individual subjects, resident strains are often retained for extended periods and only occasionally replaced [4,5], despite frequent exposure to potential colonizers, such as 'foreign' *Escherichia coli* strains [6]. Among individual subjects, taxonomic composition of the gut microbiota is highly individual, as evidenced by community profiles from 16S rRNA amplicon sequencing and analyses at the strain-level [7]. This variation among microbiomes of different individuals, shaped by host and environmental factors [2,8], may itself be a key determinant of who becomes colonized by which newly incoming strain, both early on in life and during later strain turnover. In support of this idea, various mechanisms have been identified by which interactions with resident microbiota can affect population growth of individual strains, such as nutrient competition [10], crossfeeding [11] and direct inhibition [12]. Thus, variable taxonomic composition may result in variation of these ecological interactions and, in turn, variable population growth of incoming strains. Experiments in mice support this idea: colonization success for the same strain can vary across different microbiomes [13]. Furthermore, different strains within a given species often have different phenotypes relevant for colonisation, such as nutrient preferences [14]. Some of these strain-specific traits may be advantageous in some microbiomes but not in others. This means inter-individual microbiome variation potentially determines both absolute population growth of individual strains, and the relative performance of different strains within a given species. However, testing this idea directly in human microbiomes and identifying the underlying ecological drivers is challenging.

Here, we ask how absolute and relative performance of different strains of a key commensal species vary across different gut microbiome samples, including resident microbiota and abiotic components [15]. To tackle this question, we cross-inoculate *E. coli* strains from different healthy people across their respective microbiome samples, before measuring variation of population growth depending on strain-to-strain and sample-to-sample differences. Quantifying this variability is important for our basic understanding of microbial diversity. For example, if average population growth of focal *E. coli* strains varies among samples from different people, then inter-individual microbiome variation may be a key driver of susceptibility to colonisation by incoming *E. coli* and its relative abundance compared to other taxa. Furthermore, if the identity of the best-performing strain varies among microbiome samples, this would suggest inter-individual microbiome variation is an important driver of microbial evolutionary diversification. This could potentially result in a pattern of local adaptation, in which average performance in naturally associated strain-microbiome combinations (sympatric) is higher than in combinations where strains are transplanted into other microbiomes (allopatric) [16,17]. Despite many tests in other organisms, including plants and animals [18–20], and microbes in other ecosystems [21–25], it remains unclear whether such patterns apply to bacteria in human microbiomes, and which ecological interactions determine this. There are also important practical applications of knowing how growth of bacteria such as *E. coli* varies among strains and microbiomes from different individuals. For example, understanding how the relative success of candidate probiotic strains varies among individual microbiomes would help to determine whether microbiome-based therapies, such as probiotics, should be personalized [26].

Directly quantifying the contributions of strain-to-strain and microbiome-to-microbiome variation, and their interaction, to bacterial population growth in natural human microbiomes has proven difficult until now. An important practical obstacle is that it is more or less impossible to measure population growth of individual strains in the gut microbiomes of healthy individuals in real time in a way that would permit this (with the same set of strains introduced into the same microbiomes in multiple replicated tests). There have been major advances in our understanding of related questions from work with synthetic communities in microcosms or gnotobiotic hosts [27–30]. However, the genetic variation within artificial communities, and differences among experimental groups in such systems, are not reflective of natural human-associated communities or real-world person-to-person variation. For example, the set of strains in an assembled community is typically not as species-rich and does not share the same history of ecological interactions as a natural community. Similarly, experiments with mice and associated microbiota have produced important insights [13,31], but leave gaps in our understanding of human-associated communities [32]. We circumvent some of these challenges by using anaerobic microcosms constituted with microbiome samples from healthy-human stool [33]. This allowed us to perform a reciprocal transplant experiment, measuring growth performance of six commensal *E. coli* isolates across the respective gut microbiome samples they were isolated from, each taken from a different individual healthy subject, with replication at the level of each strain-microbiome combination. Thus, we quantified the contributions of strain-to-strain and microbiome-to-microbiome differences to the 'ecological success' of commensal *E. coli*, interpreting ecological success or performance as the capacity to reach high abundance in the presence of a resident microbiota. We find that both absolute and relative performance of focal strains vary among microbiome samples from different people, and we identify some of the underlying intraspecific and interspecific interactions that explain this variation.

## Results

**Ecological success of *E. coli* varies among strains and microbiome samples from different individuals**

We sampled gut microbiomes from the stool of six healthy humans and from each we isolated a single *Escherichia coli* clone, representative of the most abundant resident *E. coli* strain (Methods, Supplementary Fig. 1). We then inoculated these six focal strains, tagged with a selective marker, into anaerobic microcosms prepared with each of the six microbiome samples resuspended in a basal medium, generating 36 unique focal strain-microbiome combinations. Within 24 h, all focal strains reached high abundance (Fig. 1). However, average final abundance varied among focal strains and among microbiome samples from different individuals ($F_{5,72}$=27.4, $p < 0.001$ and $F_{5,72}$=15.0, $p < 0.001$ respectively in a two-way ANOVA, Fig. 1). Furthermore, the relative performance of different focal strains varied among microbiome samples (interaction term, $F_{25,72}$=2.2, $p$=0.005). This was mostly due to differences in the magnitude of strain-to-strain variation among microbiome samples (e.g., much greater in microbiome sample M3 than M6, Fig. 1). Indeed, the rank order of focal strains was generally consistent across microbiome samples, with strains S3 and S7 generally reaching relatively high abundances (Fig. 1). Testing for evidence of local adaptation revealed no average difference between sympatric and allopatric strain-microbiome combinations (Supplementary Fig. 2a). Thus, some focal strains were generally more successful than others in terms of population growth in microcosms with a resident microbiota, but the strength of these differences and average ecological success varied from sample-to-sample.

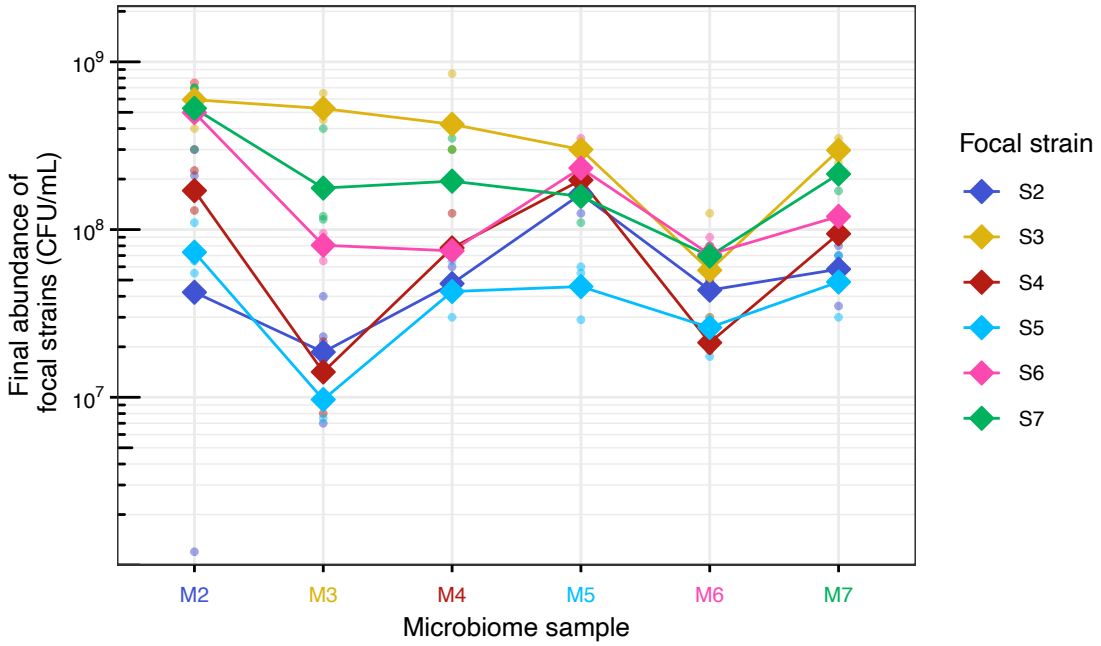


**Fig. 1: Growth performance of focal *E. coli* strains in microcosms with healthy-human microbiome samples.** Final abundance of each focal *E. coli* strain (S2-S7) in microcosms prepared with each microbiome sample (M2-M7), estimated by selective plating after 24h of anaerobic incubation. Diamonds represent the average (geometric mean) of three replicates for each strain-microbiome combination and dots show individual replicates. Lines connect the average for each strain across microbiome samples. Colors of focal strains are matched to the color of their microbiome of origin (e.g., strain 3, S3, was isolated originally from microbiome sample 3, M3).

**Focal *E. coli* strains reach consistently high abundances after biotic interactions are removed**

One possible driver of variable focal-strain growth observed above (Fig. 1) is variable interaction between focal strains and resident microbiota. If this were the case, we would expect the differences among focal strains to be weaker in the absence of resident microbiota. We investigated this using an experiment equivalent to that above, but preparing microcosms with sterilized versions of the same microbiome samples (hereafter, 'sterile' microcosms, as opposed to 'live' microcosms in the main experiment above). Here, all focal strains reached high abundance in all sterile microcosms (>$10^8$ CFU/mL, Fig. 2). Relative performance of different focal strains was stable among sterilized microbiome samples (interaction term $F_{25,72}$=0.86, p=0.66), and the range of final abundances was smaller than in the experiment above with live microcosms (ranging from $1.7 \times 10^8$ to $5.9 \times 10^8$ CFU/mL vs. $9.7 \times 10^6$ to $5.9 \times 10^8$ CFU/mL). We also found no evidence of local adaptation in these conditions (Supplementary Fig. 2b). Nevertheless, we still found average differences among focal strains and sterilized microbiome samples ($F_{5,72}$= 9.2, $p < 0.001$ and $F_{5,72}$=3.1, p=0.012 respectively). This variation of final abundances was positively associated with focal strains' maximal growth rates under equivalent abiotic conditions (i.e., sterilized microbiome sample resuspended in basal medium), measured in a separate experiment (R=0.52, p=0.001, Supplementary Fig. 3c). By contrast, there was no overall association between final abundances in sterile microcosms and in live microcosms (R=0.25, p=0.15, Supplementary Fig. 4), suggesting the drivers of focal strain performance were different in the presence versus absence of a resident microbiota. In summary, the contrast between the large variability observed in live microcosms (Fig. 1) and the invariably high abundances across strain-microbiome combinations in sterile microcosms (Fig. 2) is consistent with a critical role of the resident microbiota in determining strain-specific performance across different microbiome samples, in line with past work in this system [33].

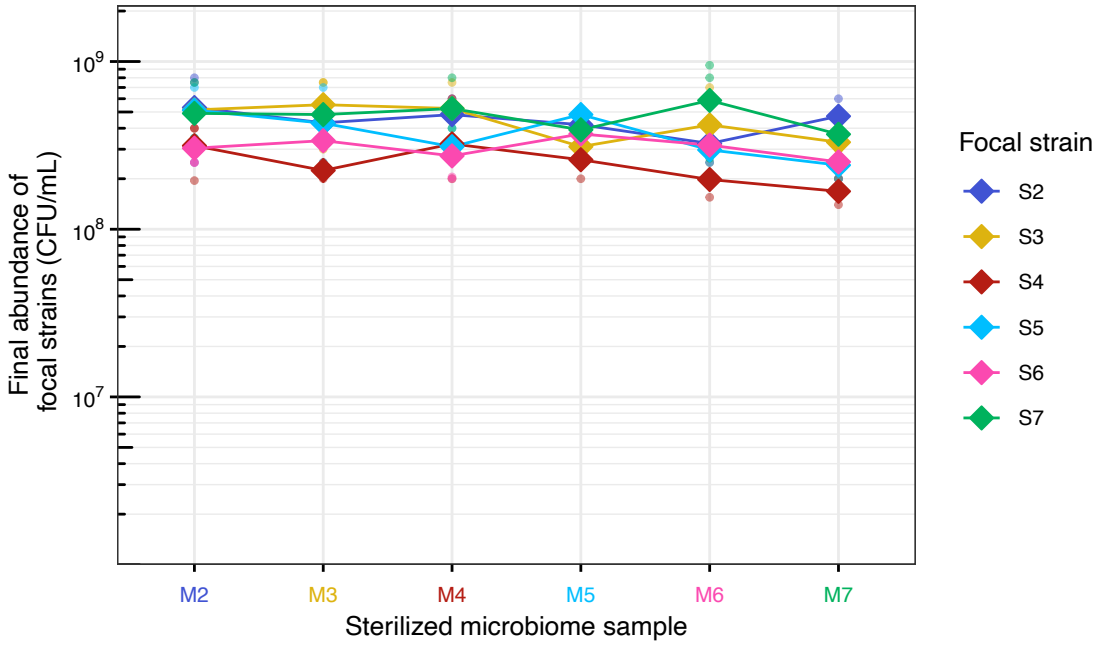


**Fig. 2: Growth performance of focal *E. coli* strains in microcosms with sterilized microbiome samples.** Final abundance of each focal strain (S2-S7) in microcosms prepared with each sterilized microbiome sample (M2-

136 M7), estimated by selective plating after 24h of anaerobic incubation. Diamonds represent the average
137 (geometric mean) of three replicates for each strain-microbiome combination and dots show individual
138 replicates. Lines connect the average outcome of each strain across microbiomes. Colors of focal strains are
139 matched to the color of their microbiome of origin (e.g., strain 3, S3, was isolated originally from microbiome
140 sample 3, M3).
141
142 **Intraspecific interactions govern *E. coli* ecological success in human microbiome samples**
143 We next tested for further evidence of interactions between focal strains and resident microbiota. First, we
144 focused on their interactions with resident *E. coli* in each microbiome sample. Total *E. coli* abundance in live
145 microcosms (including both focal strain and resident *E. coli*) varied among samples from different individuals
146 ($F_{5,72}$= 76.7, $p < 0.001$, Fig. 3). However, within each microbiome sample, total *E. coli* abundance was unaffected
147 by focal strain identity ($F_{5,72}$= 1.3, p= 0.25, main panel Fig. 3), despite considerable variation in focal strain
148 performance (Fig. 1). For example, in sample M3, average focal strain abundance ranged from $9.7 \times 10^6$ to
149 $5.3 \times 10^8$ CFU/mL (Fig. 1), but total *E. coli* abundance was relatively stable (ranging from $4.0 \times 10^8$ to $7.5 \times 10^8$
150 CFU/mL, main panel Fig. 3). This shows that in microcosms where focal strains grew relatively well, resident
151 *E. coli* was displaced. Taking focal strain abundance as a proportion of the total *E. coli* population in each
152 microcosm revealed that two strains (S3 and S7) consistently reached a comparable or greater abundance than
153 resident *E. coli* (insets Fig. 3). Furthermore, in the respective' microbiome samples of these two strains (M3 and
154 M7, where the original untagged strains S3 and S7 are the most abundant resident *E. coli* strain; see Methods),
155 all other focal strains reached relatively low frequencies (insets Fig. 3). This provides further evidence that the
156 presence of S3 and S7 was linked to suppression of other *E. coli*. Consistent with these intraspecific interactions
157 contributing to focal strain ecological success in the presence of resident microbiota, S3 and S7 reached higher
158 average absolute abundances compared to other focal strains in our main experiment (Fig. 1).

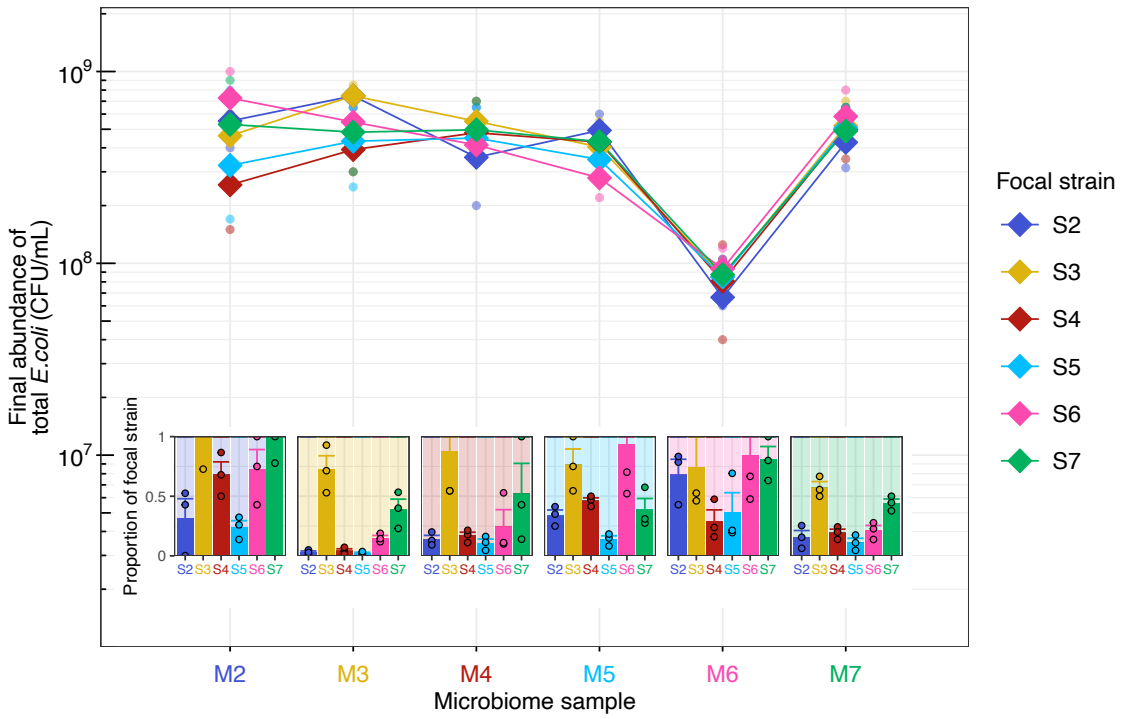

159

**Fig. 3: Total *E. coli* abundance and proportion contributed by focal strains in microcosms with human microbiome samples.** Main panel: final abundance of total *E. coli* (including focal and resident populations) for each live microcosm (Fig. 1), estimated by plating on chromatic agar without antibiotic. Dots show individual replicates, diamonds represent the average in each combination (geometric mean), and lines connect averages for each focal strain across microbiome samples. Insets: proportion of total *E. coli* made up by the relevant focal strain in each combination; dots show individual replicates and bars/error bars show mean/standard error. The y-axis scale is limited to 1; individual dots, bars and sections of error bars above 1 due to noise of the method are not displayed. The background colors in lighter shades represent the corresponding most abundant resident strain (e.g., yellow background in microbiome sample 3, M3, corresponds to the original untagged strain 3, S3).

Having observed that in live microcosms, S3 and S7 were the most successful focal strains in terms of both absolute and relative final abundance compared to resident *E. coli*, we tested whether these strains also had a competitive advantage against resident *E. coli* strains in the basal medium used to prepare microcosms. This was not the case. Instead, competitiveness in basal medium was associated with relatively rapid growth in these abiotic conditions (Supplementary Fig. 5c). Together, these results suggest ecological success in live microcosms was associated with displacement of other *E. coli* strains, but this was not driven by variable intrinsic growth capacities in the basal medium used to prepare the microcosms.

**Focal-strain private nutrient niche size does not translate to ecological success**

A possible driver of intraspecific competition in live microcosms is nutrient exploitation by focal strains relative to resident *E. coli*. We investigated this by testing for differences in the metabolic phenotype of each focal strain, monitoring biomass production across 95 single-carbon-source environments (Methods, Supplementary Fig. 6). This revealed focal strains had distinct profiles of substrate use (Fig. 4a, b). We next investigated whether different metrics describing these substrate utilization profiles were positively associated with focal-strain ecological success. This was not the case for niche size (number of substrates supporting biomass production above a threshold), which was comparable among all focal strains except S3. Despite being the most successful in terms of population growth among human microbiome samples (Fig. 1), S3 could use fewer substrates than other strains (43 vs. mean ± s.d. : 53.8 ± 0.9 for other focal strains, boxes above the x-axis, Fig. 4c). Similarly, while focal strains differed in terms of average biomass produced on viable substrates ($F_{5,10}$=4.5, p=0.02, Fig. 4c), S3 showed relatively weak growth compared to other strains. Finally, we considered a last metric potentially more relevant in the microbiome context where focal strains compete with resident conspecifics. For each focal strain, we assessed the size of the 'private niche' relative to the most abundant resident *E. coli* strain in each microbiome sample, taken as the number of carbon sources the focal strain could use that the resident strain could not use (see Methods). For example, S3 could use D-malic acid, D-raffinose and sucrose but S2 could not use (Fig. 4a), potentially reflecting a niche in microbiome sample M2 exploitable by focal strain S3 and inaccessible to competing resident strain S2. Focal strains' private niche size ranged between 2 and 16 substrates (Fig. 4d), but it was not the case that the private niche was largest in strain-microbiome combinations where the focal strain was relatively successful. For example, the private niche was largest for most strains in sample M3

198 (where S3 was the most abundant resident strain), but for S2, S4 and S5 this was the sample supporting the least
199 growth (Fig. 1). Similarly, S3 and S7 were the most successful strains (Fig. 1) but had relatively small private
200 niches in most combinations (Fig. 4d; Supplementary Fig. 7). In summary, focal strains varied in their metabolic
201 phenotypes across single-carbon-source environments, resulting in variable private niche size relative to
202 different resident strains, but this was not positively associated with their ecological success.

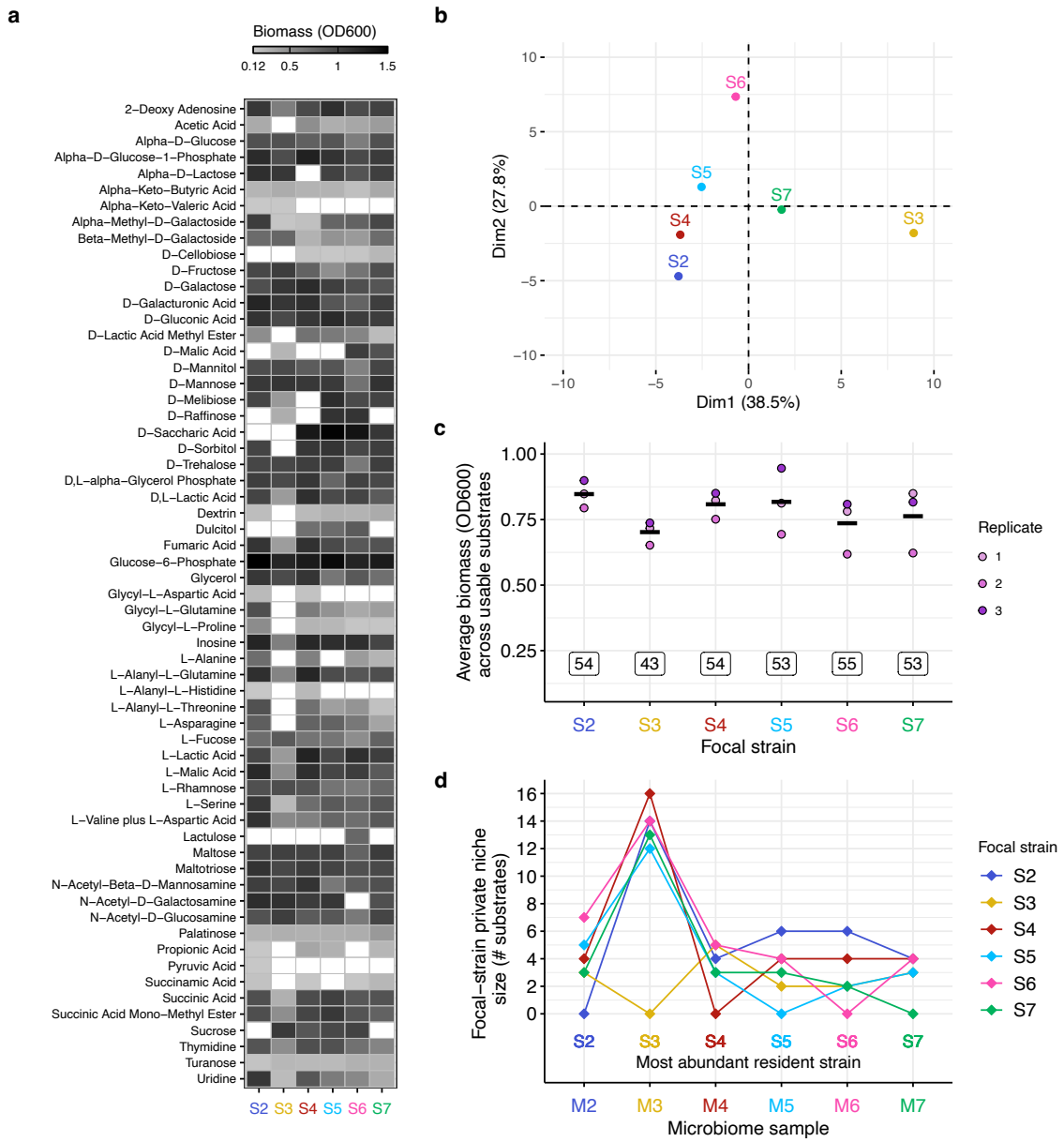


203

204 **Fig. 4: Metabolic profiles of focal *E. coli* strains across single-carbon-source environments. a** Biomass produced
205 after 24h of incubation (approximated by optical density at 600 nm, OD600) by each strain (columns) with each
206 substrate (rows, alphabetical order). The grey shade in each cell reflects mean OD600 from three replicates (see
207 legend on top), except in cases where biomass production was negligible (i.e., mean minus standard error <0.1,
208 see Methods and Supplementary Fig. 6), displayed in white. Only substrates used by at least one strain are
209 shown. **b** Principal component analysis of the metabolic profiles displayed in (a). **c** Average biomass produced
210 by the six focal strains across their respective usable substrates. Each dot correspond to one replicate and the

211 mean is shown with a crossbar. Boxes above the x-axis give the number of usable substrates for each strain. **d**
212 Size of the private niche (computed based on the binarized version of the data shown in panel a) for each focal
213 strain (see legend at right) in each microbiome sample (x-axis) where it faces the most abundant resident *E. coli*
214 strain as main competitor (labeled above the x-axis; see Methods). Note that in sympatric combinations, focal
215 and resident strains are the same, so the size of the private niche is 0. Lines connect the outcome for each focal
216 strain across microbiome samples.
217
218 **Direct antagonism among *E. coli* strains is weakly linked to ecological success in human microbiome samples**
219 Another way *E. coli* strains may compete with each other is through bacterial warfare, for example via
220 production of bacteriocins. Bacteriocins are toxins produced by a subpopulation under conditions of stress and
221 typically active against closely related bacteria [12,34]. To investigate this, we first mined focal-strain genome
222 assemblies for putative bacteriocin loci. This revealed various bacteriocin gene clusters, with individual strains
223 carrying up to three (Fig. 5a), all located on plasmids except for microcin H47, encoded on the chromosome of
224 S7. Of the three gene clusters carried by S7, one was shared with S3 and no other strain. This gene cluster
225 encoded colicin E1 and its cognate immunity gene and was located on small multicopy plasmids that were similar
226 across the two genomes (Supplementary Fig. 8). We next tested for detectable inhibitory phenotypes, first using
227 an agar overlay assay with K12-MG1655 as the indicator strain. We found S3 and S7 had relatively strong
228 inhibitory phenotypes (Fig. 5b), in line with the ability of these two strains to suppress other *E. coli* strains in live
229 microcosms (insets Fig. 3). Next, we performed the same assay across all pairwise focal-strain combinations
230 (note each focal strain also represents the most abundant resident strain in one of the six microbiome samples;
231 for example, S3 was the most abundant resident *E. coli* strain in M3). This supported inhibition of S2 and S4 by
232 S3 and S7 (Fig. 5c). These inhibition patterns were stronger upon SOS-response induction (Supplementary Fig.
233 9a), known to regulate bacteriocin production [35]. While a similar phenotype could potentially be attributed to
234 bacteriophages, spotting dilutions of the supernatants did not reveal individual plaques, but rather gradually
235 fainter inhibition patterns, consistent with toxin activity (Supplementary Fig. 9b). This led us to hypothesize that
236 colicin E1 —the only bacteriocin uniquely encoded by S3 and S7— underlies intraspecific competition in our
237 experiment. We tested this by introducing the ColE1 plasmid into S2 (the ColE1 plasmid was putatively
238 mobilizable; we moved it to S2 by agar mating with S3, mediated by an IncF plasmid carried by S3; see Methods).
239 The S2-ColE1-transconjugant displayed both immunity and inhibitory phenotypes (Supplementary Fig. 10),
240 supporting the role of the ColE1 plasmid in mediating direct antagonism. However, acquisition of the ColE1
241 plasmid did not increase the ecological success of S2 in live microcosms produced with microbiome samples M2,
242 M3 and M4 (Supplementary Fig. 11a). Instead, transconjugants performed marginally worse than the original
243 strain S2, which may be explained by a slightly reduced growth rate upon plasmid acquisition (Supplementary
244 Fig. 11b). In summary, the two best-performing strains in live microcosms encoded putative bacteriocins and
245 showed an inhibitory phenotype on agar, but when we tested the impact of the colicin plasmid mediating this
246 effect for another strain in live microcosms, it did not boost its ecological success.

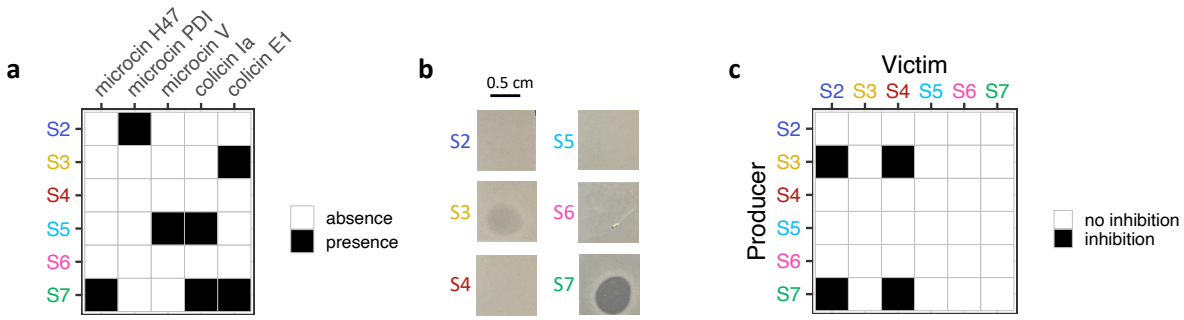


**Fig. 5: Bacteriocin gene clusters and inhibitory phenotypes among focal strains. a** Characterized bacteriocin genes identified in the genome assemblies of the six *E. coli* strains. Putative bacteriocin-associated gene clusters were first identified with BAGEL4, and then manually curated based on their functional characterization (Methods). **b** Inhibition of indicator strain *E. coli* K-12 MG1655 in overlay agar by sterile filtered supernatant of stationary-phase cultures from each focal strain (labelled to the left of each subpanel). Inhibition is visible in some combinations as a clearance zone. **c** Reciprocal inhibition matrix. Here the same type of assay as in panel (b) was done with each strain-strain combination (supernatant from "Producer" strain spotted onto a lawn of "Victim" strain; inhibition recorded if there was a visible clearance zone).

**Interspecific interactions that inhibit *E. coli* via culture acidification partly explain variable average focal strain performance among samples from different individuals**

Aside from resident *E. coli*, the relative abundances of other taxa may vary among microbiome samples, potentially contributing to the observed sample-to-sample variation of focal strain performance in our main experiment. Consistent with this, when we profiled the resident community in each sample (prior to cultivation in microcosms), taxonomic composition varied among samples (Fig. 6a, Supplementary Fig. 12). In particular, microbiome sample M6 had a high proportion of *Enterococcaceae* (27%, brown, Fig. 6a) —not detected in other samples except M4, where its relative abundance was only 0.3%— and a relatively high proportion of *Bacteroidaceae* compared to other samples (26% vs. mean ± s.d.: 7% ± 3% in other samples, lightest pink, Fig. 6a). M6 also had a relatively low abundance of resident *E. coli* prior to cultivation, shown by both 16S sequencing (all reads assigned to *Enterobacteriaceae* were of a single amplicon sequence variant, ASV, assigned to *E. coli* and made up 0.02% in M6 vs. mean ± s.d.: 0.06% ± 0.01% in other samples; Supplementary Fig. 12b) and plating (Supplementary Fig. 13a). In terms of total bacterial diversity, M6 was less diverse than other samples (Fig. 6b). The distinctiveness of this sample was further supported by final abundances after our main experiment: total bacterial abundance was approximately 50% lower in microcosms produced with M6 compared with other samples (measured by flow cytometry, Fig. 6c). This trend was even stronger for *E. coli*, in that final total *E. coli* abundance was approximately six-fold lower in microcosms produced with M6 compared with other samples (Fig. 3, Supplementary Fig. 13b), and average focal strain performance was lowest in M6 (Fig. 1). Thus, microcosms prepared with microbiome sample M6 were the least favourable for microbial growth and particularly for *E. coli*, including our focal strains.

We next investigated possible causes of the relatively low focal-strain abundances reached in M6 microcosms (Fig. 1). Given this effect was not observed in sterile microcosms prepared with sample M6 (Fig. 2, Supplementary Fig. 3b), we hypothesized the relatively unfavorable conditions in M6-microcosms emerged during incubation of the resident microbiota. To test this, we took supernatant from microcosms prepared with each sample and cultivated in the same conditions as the main experiment (but without introducing focal strains), then monitored growth dynamics of each focal strain in each supernatant. Supernatant from M6-microcosms supported much less focal-strain growth than the other supernatants (top panel Fig. 6c, Supplementary Fig. 14 and Supplementary Fig. 15), consistent with the resident microbiota in that sample generating a relatively unfavorable environment for focal strains upon incubation. Because the most striking feature of the M6 resident microbiota was the high abundance of *Enterococcaceae* (three ASVs all assigned to the *Enterococcus faecium* species), which produces lactic acid during fermentation of carbohydrates [36], we hypothesized acidification of the microcosm environment contributed to the unfavourable conditions in M6 microcosms. Three pieces of evidence are consistent with this. First, the pH of M6-microcosm supernatant was considerably lower than that from other microbiome samples (colored-squares in top panel Fig. 6d). Second, the growth impairment could be reversed by extraneous alkalinization: neutralizing the pH of the M6-supernatant with sodium hydroxide restored growth of all focal strains (bottom panel Fig. 6d). Third, going back to aliquots from the end of our main experiment (Fig. 1) and measuring pH revealed that all M6-microcosms had a lower pH than microcosms prepared with other microbiome samples (on average 5.4 in M6 vs. mean ± s.d. 6.1 ± 0.2 in other samples, Supplementary Fig. 16), consistent with this process occurring in our main experiment. In summary, the microbiota in one sample had a distinctive taxonomic composition, resulting in acidification of the microcosm environment and relatively poor growth of *E. coli*. This process helps to explain the microbiome-to-microbiome variation observed in our main experiment (Fig. 1).

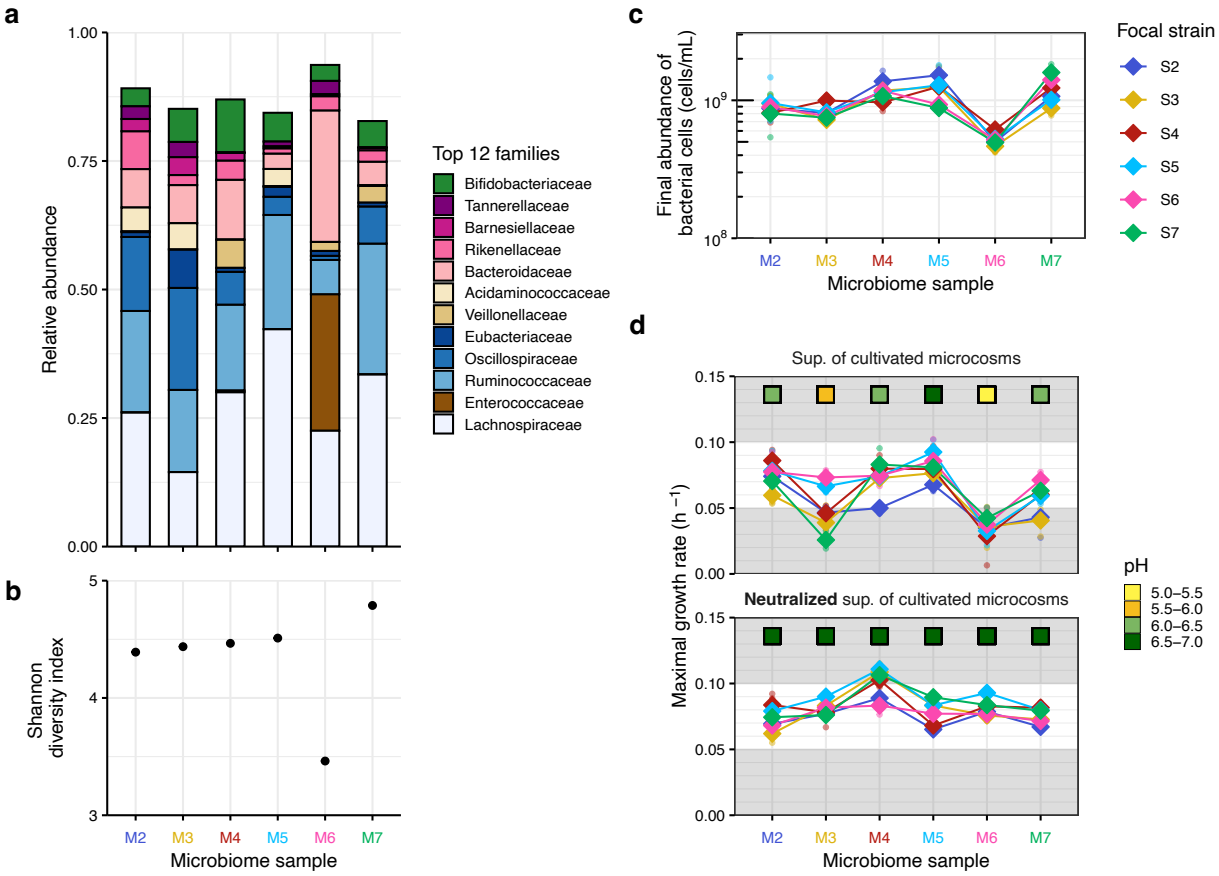


**Fig. 6: Distinctive taxonomic composition is associated with impaired *E. coli* growth due to culture acidification.** **a** Taxonomic composition of microbiota from the six samples before cultivation. Relative abundance of the twelve most abundant families across samples, ordered and colored based on phylum (from top to bottom: Actinobacteriota in green; Bacteroidota in pink shades; and Bacillota, further distinguished by class: Negativicutes in beige shades, Bacilli in brown and Clostridia in blue shades). Within phylum, families are ordered by ascending abundance. **b** Alpha diversity (Shannon diversity index) for each microbiome sample before cultivation. **c** Final total bacterial abundance in the live microcosms estimated by flow cytometry. Diamonds represent the average (geometric mean) of three replicated microcosms (points for each focal strain and microbiome sample combination) and lines connect the average outcome for microcosms prepared with a given focal strain across microbiome samples. **d** Maximal growth rate of each focal strain in supernatants of cultivated microbiome-only microcosms (prepared with the same six microbiome samples and incubated as in Fig. 1, but without inoculating focal strains) and in corresponding supernatants, neutralized to pH 6.5-7.0. The colored squares on the top show approximate pH of spent medium in each group on a scale from 5 to 7 (see Methods). The background shaded areas serve as visual reference to compare y-range spanned across panels. The white area corresponds to the range of maximal growth rates reached by the focal stains in sterile microcosms (0.05 to 0.10 $h^{-1}$, Supplementary Fig. 3b, bottom subpanel).

316 ## Discussion

317 We aimed to test whether variation of the human gut microbiome among samples from different individuals
318 translates to variable ecological interactions with individual strains of a key commensal species. To this end, we
319 performed a reciprocal transplant experiment using gut microbiome samples from healthy humans, cross-
320 inoculating strains of *E. coli* among the samples and testing for variable population growth and interactions with
321 resident microbiota. We found that both absolute and relative population growth of focal *E. coli* strains varied
322 among microbiome samples from different people. This provides evidence that person-to-person gut
323 microbiome differences are a key driver of the ecological success of incoming strains. We identified ecological
324 processes that explain much of that variation: variable intraspecific competition (with two of the tested strains
325 being relatively successful at displacing other *E. coli* strains, either when introduced into other samples or when
326 other strains were introduced into their home sample) and interspecific interactions (with one microbiome
327 sample impairing *E. coli* growth via culture acidification).

328 An important implication of our results is that average growth of commensal *E. coli* varies among
329 samples from different people. This suggests inter-individual microbiome variation is a key driver of
330 susceptibility to colonisation by incoming *E. coli* and its relative abundance compared to other taxa. This matters
331 because, although individuality in terms of taxonomic composition of human microbiomes has been widely
332 documented [7,37], the functional consequences of this are not well understood. One exception is the
333 substantial evidence that dysbiosis (disruption of the microbiota) influences ecological success of incoming
334 pathogens such as *Clostridioides difficile* [38]. Our results show that an even more common form of microbiome
335 variation, among samples from healthy individuals, also has functional consequences in terms of the ecological
336 success of incoming commensal strains. Much of this variation in our experiment was explained by variation of
337 taxonomic composition among samples, with the most distinctive resident community (in sample M6) causing
338 acidification of the local environment below pH 5.5, largely overcoming the carbonate- and phosphate-buffering
339 of the basal medium, and in turn inhibiting growth of *E. coli*. Acidification due to microbial activity and
340 downstream impacts on performance of other strains are likely to be prevalent in nature. For example, physical
341 conditions vary across gut compartments [40], some common taxa contribute to mild acidification (pH 5.5-6),
342 and other taxa, including *E. coli*, thrive under close-to-neutral conditions (pH 6.5-7) [41,42]. The extent and
343 dynamics of acidification probably differ among individual microbiomes, due for example to dietary differences
344 [43], and between natural settings and our microcosm system. Nevertheless, acidification may be a common
345 mechanism by which person-to-person microbiome variation translates to variable performance of incoming
346 strains. More generally, pH variation has been found to play a key role in microbial community composition in
347 natural environments such as soil [39]. Besides acidification, there are likely other mechanisms by which
348 taxonomic composition can determine the growth potential of incoming strains. Our data are consistent with
349 this, in that sample M6 was not the only source of microbiome-to-microbiome variation: in a version of the
350 analysis above for Fig. 1, but excluding sample M6, we still detected variation of focal strain abundance among
351 strains and microbiome samples (main effect of strain: $F_{5,60}$=25.0, $p < 0.001$ and microbiome: $F_{4,60}$=9.9, $p < 0.001$;
352 interaction term: $F_{20,60}$=1.9, $p$ =0.031). The variable intraspecific interaction we detected (insets Fig. 3) enabled
353 us to exlpain some of this remaining variation among strains and samples.

354 A second important implication of our results is that differences among strains of *E. coli,* in terms of
355 their growth performance in human microbiome samples, vary strongly among samples from different healthy
356 humans (strain-to-strain variation lowest in sample M6 and highest in sample M3), despite a generally consistent
357 strain rank order among samples. From an applied perspective, this suggests that testing candidate probiotic
358 strains in several different microbiome samples is valuable. This is because some strains performed well across
359 the samples we tested, such as S3 and S7, but others performed well in some samples and poorly in others, such
360 as S4 and S6. If we had only tested one or two microbiome samples, we could have mistakenly inferred that all
361 four of those strains had similar average growth performance in human microbiome samples. Thus, in our
362 system S3 and S7 embody desirable characteristics for a probiotic strain: they grow relatively well in all tested
363 microbiomes (Fig. 1) and they can restrict growth of foreign strains in their home microbiome (insets Fig. 3).
364 From a fundamental perspective, the consistency of strain performance rank order and the lack of a signature
365 of local adaptation advances our understanding of the extent to which strains are matched to individual
366 microbiomes. This is inconsistent with the idea that the most abundant resident *E. coli* strain from a given
367 microbiome performs relatively well in that microbiome compared to 'foreign' strains, or that the home
368 microbiome of a given strain is relatively favourable for that strain compared to other microbiomes. We do not
369 exclude the possibility that a stronger signature of local adaptation would be found in other species. For
370 example, other species such as strict anaerobes may be subject to restricted dispersal compared to aerotolerant
371 microorganisms [44], potentially playing a decisive role in the emergence of local adaptation [16]. Thus, future
372 work increasing the number of tests for local adaptation in human microbiomes may reveal a picture similar to
373 that indicated by previous work with microbes in other ecosystems, where signatures of local adaptation are
374 sometimes detected [23–25] and sometimes not [21,22].
375 Our results provide new information about the ecological processes driving competition among
376 different strains of the same species in human-associated microbial communities. Experiments with mice and
377 communities assembled in vitro suggest that nutrient blocking by conspecifics in the resident microbiota
378 suppresses establishment of an incoming strain [10,45]. Our results, in a system with microbial communities
379 sampled directly from humans and thereby accounting for some interactions and complexity not captured by
380 other approaches, challenge the generality of this finding. In human microbiome samples, we found metabolic
381 profile, and more specifically private niche size of an individual strain relative to the most common resident
382 conspecific, is not positively associated with ecological success. While we do not exclude a role for nutrient
383 competition more generally, our results support an additional or even stronger role for direct antagonism,
384 possibly mediated by colicin production. Successful strains produced a colicin achieving detectable inhibition of
385 competitors. Despite this, acquiring the plasmid and the corresponding inhibitory phenotype did not boost
386 ecological success of another strain in live microcosms. Note this does not rule out colicin E1 contributing to the
387 ecological success of strains S3 and S7. The S2-ColE1-transconjugant (Supplementary Fig. 10) may have
388 expressed the colicin, or been affected by its expression, differently in live microcosms compared to the other
389 strains that naturally carry the plasmid encoding this colicin. Indeed, colicin expression is regulated by the DNA
390 damage response regulatory system (SOS), interconnected with the carbon storage regulator (Csr) system [46].
391 Therefore, it is conceivable that bacteria with different genetic backgrounds would not express the same colicin

392 under the same circumstances. These results therefore open new directions for work about colicins, for example
393 investigating the conditions in which colicins are deployed by *E. coli* populations competing in the gut.
394 Finally, our results also open up new questions about the impact of *E. coli* population structure on
395 colonization success of different gut microbiome samples by individual strains. For example, it is possible that in
396 nature some variability of ecological performance among strains is linked to their phylogenetic relatedness, with
397 more closely related strains potentially sharing some phenotypes [48]. Our results are in some ways consistent
398 with such a trend, in that the two relatively successful strains S3 and S7 belong to the same phylogroup and
399 share some phenotypes (metabolic profile and direct inhibition). Presence of the plasmid encoding colicin E1 to
400 which we attributed the direct inhibition phenotype in two relatively closely related strains may be a coincidence
401 but may also result from a stable long-term association of this plasmid with a clonally expanding lineage [47].
402 However, we would need a much larger number of strains to properly assess the role of phylogenetic structure
403 in colonisation of human samples. Furthermore, although working with samples from different people allowed
404 us to investigate drivers of ecological success among independent human-associated microbial communities, a
405 different experimental design and scale would be needed to quantify the contribution of the identity of the
406 donor to the observed sample-to-sample variation. To do this, more than one sample per individual would be
407 required and, ideally, metadata to allow associations with host factors such as age, diet or immune status to be
408 tested.
409 In conclusion, we used a reciprocal transplant experiment to cross-inoculate strains of a key commensal
410 species across microbiome samples from different healthy humans. This allowed us to go beyond past work with
411 assembled communities and mice, by quantifying variation caused by differences among strains and microbiome
412 samples in replicated experiments with natural human samples. We detected both intraspecific competition
413 between focal and resident *E. coli* strains, and variable interactions between *E. coli* and other species, such as
414 the inhibition resulting from acidification by the taxonomically distinctive community in microbiome sample M6.
415 Our results therefore also advance our knowledge from the many studies that have documented person-to-
416 person microbiome variation, by revealing some of the ecological effects of this common form of variation. This
417 in turn improves our understanding of what makes a given strain succeed in an individual person's microbiome,
418 relevant for our basic knowledge of microbial diversity and microbiome-based therapies such as probiotics.
419 Specifically, our finding that microbiome composition can decisively influence the success of newly incoming
420 strains indicates, as already established for dysbiosis, that data on community composition may eventually
421 inform improved predictions about susceptibility to colonisation by pathogens or probiotic strains.

422 # Material and methods

423 **Sampling, processing and 16S profiling human microbiome samples**

424 Stool samples were collected at the Department of Environmental Systems Science of ETHZ on the 17th of March
425 and the 24th of Mai 2022 from anonymous above-18-year-old healthy donors, who had a body mass index
426 between 19 and 25, were not recovering from surgery, had not taken antibiotics in the previous six months, and
427 did not test positive for SARS-CoV-2 in the previous two months. The sampling protocol was approved by the
428 ETHZ Ethics Commission (EK 2020-N-150). Each volunteer provided one stool sample in a sealed box supplied
429 with an AnaeroGen 2.5L sachet (Thermo Scientific) to maintain an anaerobic atmosphere. We processed the
430 samples under anaerobic conditions in an anaerobic chamber (Coy Labs, USA) within six hours. We resuspended
431 stool samples 10% *w*:*v* ratio in peptone wash, prepared as previously described (the following components in
432 water, in g per liter: 1.0 peptone from casein, 0.5 L-cysteine, 0.5 bile salts and 0.001 resazurin) [33]. We then
433 froze the resulting faecal slurries with 10% glycerol and stored them at -80°C. For this project, we selected six
434 samples randomly. These faecal slurries include a resident microbiota and abiotic components and are referred
435 to as 'microbiome' samples hereafter. Because we were unable to isolate *E. coli* (see below) from one of them
436 (M1), we excluded it and replaced it with another (M7). We therefore performed all experiments with
437 microbiome samples M2-M7.

438 For 16S rRNA gene sequencing, we sent 2 mL aliquots from each sample to Microsynth AG, Switzerland,
439 for DNA extraction, amplification of the V3V4 region of the 16S rRNA gene using primers 341F
440 (5'-CCTACGGGNGGCWGCAG-3') and 805R (5'-GACTACHVGGGTATCTAATCC-3') [49], and sequencing on an
441 Illumina MiSeq instrument. We obtained 92000 +/- 11000 (mean ± s.d.) reads per sample. We used the package
442 DADA2 v. 3.18 [50] to inspect quality profiles, filter and trim reads and obtain ASVs following the workflow
443 described in [51] and using SILVA nr.99 v.138 dataset. Filtering resulted in a total of 81000 +/- 10000 (mean ±
444 s.d.) reads per sample to which an ASV was assigned. With the obtained ASV table and corresponding taxa table,
445 we used the R package phyloseq v 1.46, to create a phyloseq object and downstream analyses and plots. We
446 quantified alpha and beta diversity using the functions 'plot_richness' with measure 'Shannon' and 'distance'
447 with method 'bray', respectively.

448

449 **Isolation, tagging and sequencing of focal *E. coli* strains**

450 To isolate the focal *E. coli* strains from the samples, we plated faecal slurries at several dilutions on chromatic
451 Mueller-Hinton (MH) agar (Liofilchem, Roseto degli Abruzzi, Italy). From each sample, we chose randomly one
452 purple colony, inoculated it in lysogeny broth (LB, Sigma-Aldrich) and added 25 % glycerol for preservation
453 at -80 °C. We confirmed that picked colonies were *E. coli* by amplifying and sequencing a fragment of *dnaJ,* using
454 primers DN1-1F (5'-GATYTRCGHTAYAACATGGA-3') and DN1-2R (5'-TTCACRCCRTYDAAGAARC-3') [52]. Because
455 multiple *E. coli* strains can co-exist in the same microbiota [53,54], we tested whether the picked colony isolates
456 represented the most abundant *E. coli* strain in each sample by repetitive element palindromic PCR (rep-PCR),
457 using primers REP1R (5'-NNNGCGCCGNCATCAGGC-3') and REP2R (5'-ACGTCTTATCAGGCCTAC-3') [55]. This
458 approach allowed us to establish the fingerprint (corresponding to a band pattern on electrophoresis gel)
459 characteristic of each of the six isolated *E. coli* clones and compare it to that of nine other random colonies from

460 each corresponding sample. In five cases, the isolated *E. coli* clone showed a fingerprint matching with 9/9 other
461 colonies from the same sample, and in one case (sample M6) it matched with 8/9 other colonies, indicating that
462 in each sample, the isolated clone represented the most abundant *E. coli* resident strain.

463 To be able to track these six focal strains (S2-S7) upon inoculation into gut microcosms, where there is
464 a resident microbiota including other *E. coli* cells, we tagged each of them with a selective marker. We did this
465 by electroporating the non-mobilizable plasmid pACYC184 (New England Biolabs), which encodes
466 chloramphenicol resistance [56,57]. Comparing final abundance of each focal strain in sterile microcosms
467 assessed by plating on agar with and without antibiotics (see below) indicated that the plasmid was stable in our
468 experimental conditions (based on pairwise t-tests, abundance differed in only 2/36 combinations, and in
469 different directions: M2, S3 $t(2) = -8.00$, $p=0.015$ and M3, S7 $t(2) = 5.64$, $p=0.030$, but both p-values were >0.05
470 upon adjustment for multiple testing with Bonferroni correction). Furthermore, comparing growth dynamics
471 and competitive fitness of original untagged strains vs. their tagged counterparts in basal medium
472 (Supplementary Fig. 3a and Supplementary Fig. 5b respectively) revealed a small cost of bearing the plasmid,
473 which was comparable among strains and therefore unlikely to confound other causes of strain-to-strain
474 variability in our main microcosm experiments.

475 We sequenced the whole genome of both the original untagged and the tagged version of the focal
476 strains (with short-read sequencing and both short- and long-read-sequencing, respectively). DNA extraction
477 and sequencing were performed at the Institute of Medical Microbiology of the University of Zurich (IMM, UZH).
478 DNA was extracted with the Maxwell RSC Blood DNA Kit (Promega, Madison USA). Libraries were prepared with
479 the QIAseq FX DNA Library Kit (QIAGEN, Hilden, Germany) for 150-paired-end sequencing on an Illumina
480 NextSeq1000, and with the Rapid Barcoding Kit 24 V13 (Oxford Nanopore Technologies, Oxford, UK) for
481 sequencing with the Minion R.9.3 flowcell on a GridION (Oxford Nanopore Technologies, Oxford, UK).
482

483 **Anaerobic gut microcosms**

484 We quantified growth performance of the focal strains (S2-S7) among microbiome samples (M2-M7) by
485 cultivating them in anaerobic microcosms. We prepared anaerobic 8mL-microcosms in 15mL screw-cap tubes
486 (Sarstedt), containing 0.5 mL microbiome sample (either thawed, or thawed and sterilized by autoclaving for the
487 sterile-microcosms experiment) and 7.5 mL of basal medium, prepared as previously described (resuspending
488 the following components in water, in g per liter: 2.0 peptone from casein; 2.0 tryptone, 2.0 yeast extract, 0.1
489 NaCl, 0.04 $K_2HPO_4$, 0.04 $KH_2PO_4$, 0.01 $MgSO_4x7H_2O$, 0.01 $CaCl_2x6H_2O$, 2 $NaHCO_3$, 1.8 Tween 80, 0.005 hemin, 0.5
490 L-cysteine, 0.5 bile salts, 2 starch, 1.5 casein, 0.001 resazurin; adjusting the pH to 7; autoclaving and finally adding
491 0.001 g per liter menadion) [33]. We made three replicate microcosms in each combination of focal strain and
492 microbiome sample, giving 108 microcosms in total for the live- and sterile-microcosm experiments. We added
493 focal strains (tagged versions) after diluting independent overnight cultures (incubated at 37 °C statically and
494 anaerobically in 200 µl basal medium), aiming to achieve an inoculum density between $10^4$ and $10^5$ CFU/mL. We
495 chose this inoculum density to start with comparable amounts of focal and resident *E. coli* (Supplementary Fig.
496 13a). We incubated microcosms at 37 °C, statically and anaerobically for 24 h. We assessed abundance of focal
497 strain and total *E. coli* by sampling 200 µl from well-mixed microcosms and spot-plating dilutions on chromatic

498 MH agar plates supplemented with 25 µg/mL chloramphenicol and without antibiotics respectively. In live
499 microcosms, effective starting densities varied among focal strains ($F_{5,72}$=52.85, $p$<0.001, ranging between
500 $2 \times 10^4$ and $8 \times 10^5$ CFU/mL, Supplementary Fig. 17a). A separate experiment, in which we inoculated one focal
501 strain at different densities into three different microbiome samples, indicated that within this range, final
502 abundance was independent of inoculum density (Pearson's correlation coefficient R=0.23, p=0.25,
503 Supplementary Fig. 17b). Therefore, we took final abundance as a measure of focal strain growth performance.
504 In a separate experiment, we estimated initial and final abundance of resident *E. coli* in the absence of tagged
505 focal strains (Supplementary Fig. 13), preparing and cultivating microbiome-only microcosms in the same way
506 as we did for the live microcosm experiment, but without inoculating focal strains. Here as well, we made three
507 parallel replicates, giving a total of 18 microcosms. For all microcosm experiments, we supplemented aliquots
508 or the whole volume of the cultivated microcosms with 10% glycerol and stored them at -80 °C for further use.
509
510 **Downstream measurements and further use of cultivated gut microcosms**
511 We estimated total bacterial abundance in aliquots from live microcosms using flow-cytometry (Fig. 6c). We
512 thawed aliquots of the 108 microcosms, diluted them 1:1000 in 200 µl phosphate-buffered-saline (PBS) and
513 stained cells with the addition of 5 µl SYBR Green (Invitrogen, Thermo F. Scientific). We used a Novocyte 2000R
514 (ACEA Biosciences, San Diego, CA, USA) with the following parameters: 50 µl flow rate, 14.6 core diameter and
515 100'000 events recorded per sample. We made pH measurements by thawing the 18 microbiome-only
516 microcosms and using the pH-Fix 2.0-9.0 test-strips (Macherey-Nagel). From the same microcosms we prepared
517 supernatant, removing bacterial cells by centrifugation (4000 g, 10 min) and sterile filtering with a pore size 0.2
518 µm (Filtropur S, Starstedt). After monitoring growth dynamics of the focal strains in these supernatants (see
519 below), we adjusted the pH of the remaining volume of each supernatant, by adding few microliters of 1M
520 sodium hydroxide and remeasuring, until reaching a pH of 6.5-7 (up to 6 mM sodium hydroxide in the three
521 supernatants from M6 microcosms). Finally, we also measured pH in supernatant from the 108 microcosms from
522 the main experiment, after first thawing and centrifuging them, using a portable pH-meter FiveGo F2 (Mettler
523 Toledo) (Supplementary Fig. 16).
524
525 **Quantifying local adaptation**
526 For both live- and sterile-microcosm experiments, we quantified average local adaptation, defined as the
527 sympatric-allopatric (SA) contrast [17] (Supplementary Fig. 2). The SA-contrast corresponds to the difference
528 between average focal-strain performance in sympatric strain-microbiome combinations (the six combinations
529 in which focal strains were inoculated into their home microbiome sample) vs. allopatric strain-microbiome
530 combinations (the other 30 combinations). For each data set, we tested whether the observed SA-contrast value
531 differed from the null expectation (no average difference between sympatric and allopatric combinations), by
532 first calculating the SA-contrast score in each of 1000 random permutations of the same dataset (where the
533 same 36 values as used in calculating the observed SA-contrast were randomly reassigned across strain-
534 microbiome combinations). We then assessed the probability that the observed value could have arisen by
535 chance from the proportion of randomly permuted SA-contrast scores lower than the observed result.

536

537 **Growth dynamics and pairwise competitions of focal strains**

538 To quantify population growth dynamics of each focal strain, which we did in various conditions (basal medium,
539 sterile microcosm conditions and supernatant of cultivated microbiome-only microcosms) and always
540 aerobically, we diluted independent overnight cultures (incubated at 37 °C shaking and aerobically in 200 µl
541 basal medium) 1:1'000 in 200 µl of the corresponding media in a microplate. We then incubated microplates at
542 37 °C in a plate reader (Tecan NanoQuant Infinite M200 Pro), shaking and measuring optical density at 600 nm
543 (OD600) every 15 min and during 24 h. To assess contribution of strain identity and selective marker (pACYC184)
544 to the variability of growth dynamics, we monitored growth of both tagged and untagged version of each focal
545 strain in basal medium (Supplementary Fig. 3a). In all other conditions, we characterized growth of the tagged
546 version of focal strains exclusively. To monitor growth in sterile microcosm conditions (Supplementary Fig. 3b
547 and Supplementary Fig. 14), we prepared one tube per sample containing 0.5 mL of autoclaved microbiome
548 sample and 7.5 mL of basal medium, and we let particles sediment overnight at 3 °C. We then inoculated each
549 focal strain in each sterile microcosm medium, with three replicates for each strain-microbiome combination.
550 To monitor growth across supernatants of cultivated microbiome-only microcosms (Supplementary Fig. 6d,
551 Supplementary Fig. 14), we inoculated each focal strain into three replicated supernatants from each
552 microbiome sample, prepared as described above. We estimated maximal growth rates with the R package
553 growthrates [58] by fitting a linear regression to the 8-datapoint subset (corresponding to a 2-hours window)
554 with the steepest log-linear increase. We extracted the area under the curve, which correspond to a sum of the
555 all 96 OD600 values over 24 h, with the R package growthcurver [58].

556 To quantify relative competitive fitness of the *E. coli* strains, we prepared triplicates of all strain-strain
557 combinations by diluting independent overnight cultures (incubated at 37 °C shaking and aerobically in 200 µl
558 basal medium) 1:1'000 and adding them to 200 µl of basal medium in a microplate. Thus, the competitors were
559 initially at a 1:1 ratio and an abundance of approximatively $10^5$ CFU/mL and we co-cultivated them during 24 h.
560 Each combination included an untagged and a tagged version of the strains, to enable monitoring of initial and
561 final abundance of focal strains (by enumerating CFU on agar with antibiotics) and estimation of initial and final
562 abundace of untagged strains (by subtracting CFU attributed to focal strain from total CFU enumerated on agar
563 without antibiotics). We then computed the selection rate constant with the formula $ln\,(\frac{A_f}{A_i}) - ln(\frac{B_f}{B_i})$, where
564 A corresponds to the tagged strain population and B the untagged strain population, and the subscripts i and f
565 to initial and final abundance [59].

566

567 **Whole-genome assemblies and analyses**

568 We filtered long reads with Filtlong v 0.2.1 (https://github.com/rrwick/Filtlong) by discarding reads shorter than
569 1 kb and 10% read bases with poorest quality. We generated hybrid assemblies combining short- and filtered
570 long-reads with Unicycler [60]. Despite having scaffolded the assemblies with long reads, some remained
571 incomplete, i.e. featured uncircularized contiguous sequences (contigs). We extracted assembly statistics with
572 assembly-stats v. 1.0.1 (https://github.com/sanger-pathogens/assembly-stats) (Supplementary File 1). We used
573 PlasmidHunter [61] to assign each contig to chromosome or plasmid. We annotated the assemblies with Prokka

574 v 1.14-6 [62] and constructed a pangenome with Roary v 3.13.0 [63], using the command -e mafft. We used the
575 resulting core gene alignment to construct a maximum likelihood tree with FastTree 2 [64]. We determined
576 phylogroup and sequence type of the strains with the tools ClermonTyping (http://clermontyping.iame-
577 research.center) and mlst (https://github.com/tseemann/mlst). We screened assemblies for characterized
578 *E. coli* virulence factors (including bacteriocins) with Abricate v 0.5 (https://github.com/tseemann/abricate),
579 using the database *ecoli_vf* (https://github.com/phac-nml/ecoli_vf) and default parameters (–minid 80%). Then,
580 we mined the assemblies for regions encoding putative prophages and bacteriocins clusters with PHASTER [65]
581 and BAGEL4 [66] respectively. To create a list of putative bacteriocins, we considered the areas of interest
582 identified by BAGEL4 that included a core peptide and inspected genomic context and whether core peptides
583 matched functionally characterized *E. coli* bacteriocins. Most of them did match bacteriocin genes included in
584 the *ecoli_vf* database (Supplementary File 2) or, in one case, the recently characterized gene cluster mccPDI
585 [67,68] (Supplementary Fig. 17). One core peptide—identified on the chromosome of the strains from
586 phylogroup B2 (S2, S4 and S5)— encoded the T6SS effector protein Hcp fused with extended-toxin domains
587 (Hcp-ET3-4), also found on the chromosome of the reference strain *E. coli* Nissle [69,70]. We excluded this hit
588 from the list of putative bacteriocin because it is not formally classified as such. We used clinker [71] to visualize
589 the alignments of the colicin E1 plasmids carried by S3 and S7 (Supplementary Fig. 8).
590
591 **Agar inhibition assays and conjugation of colicin plasmid**
592 We prepared bacterial lawns by diluting 200 µl of an exponential-phase culture from the indicator strain
593 (approximately $2 \times 10^8$ colony-forming-units (CFU)/mL) in 6 mL soft LB agar (0.4% *w*:*v* agarose), pouring it onto
594 LB agar plates and allowing it to dry for 30 min. We then spotted 5 µl of filter-sterilized supernatant from
595 stationary cultures of the strains to be tested. We also used a variation of this protocol, using filter-sterilized
596 supernatant of exponential-phase cultures with and without induction of the SOS response, prepared by diluting
597 stationary cultures 1:100 in LB, and incubating for 5h with and without addition of 0.5 µg/mL mitomycin C after
598 1h [35]. In the reciprocal inhibition assay, we used the focal strains (original untagged versions) as both indicator
599 and producer (Fig. 5c, Supplementary Fig. 9a). In a separate experiment, to rule out that the observed clearance
600 zones resulted from lysis by phages, we used strain K12-MG1655 lambda+ Δbor::cm [72] as producer in parallel
601 with focal strains S3 and S7 and spotted dilutions of the filter-sterilized supernatants of exponential-phase
602 cultures exposed to mitomycin C (Supplementary Fig. 9b).
603 In strain S3, the colicin plasmid hypothesized to be responsible for the observed inhibitory phenotype
604 encoded the mobilization protein MbeC and the relaxase MbeA (Supplementary Fig. 7) and was therefore
605 putatively mobilizable. S3 also carried an IncF conjugative plasmid, which encoded several resistance genes. We
606 performed a conjugation experiment with the tagged version of S2 as recipient and the original untagged version
607 of S3 as donor. We used the natural resistance to trimethoprim conferred by the IncF plasmid and the
608 chloramphenicol resistance of the recipient to select for transconjugants. We selected ten transconjugant
609 colonies and performed colony PCRs to verify that they carried the IncF plasmid (with primers IncFII_F
610 5'-CCGCATAGAAGCTGTTGCT-3' and IncFII_R 5'-TCCTGCACTTATGTTGCACAG-3') and the two original S2 plasmids
611 (IncB/O/K/Z and the IncX3, with primers IncO_F 5'-GTCCGGAAAGCCAGAAAACG-3' and IncO_R 5'-

612 CCGCCAAGTTCGACAGGAAG-3' ; IncX3_F 5'-GGGGTAACTCTTGCATCCCTT-3' and IncX3_R
613 5'-TTTCAGAGCTGCATAAGAGGCA-3' respectively). As expected, all transconjugants carried the three plasmids.
614 Furthermore, we screened for colE1 plasmid carriage (with primers colE1_F 5'-AAGCCCGTAAAGAAGCGGAA-3'
615 and 5'-ATTTCGTTTTCCAGCGAGCG-3') and found that 1/10 transconjugants also carried the colE1 plasmid. We
616 named this transconjugant S2t1 and, as control to discriminate possible phenotypic effects conferred by
617 acquisition of the IncF plasmid rather than the colE1 plasmid, we picked one of the other transconjugants
618 without colE1 plasmid (S2t2).
619
620 **Metabolic phenotyping across single-carbon-source environments**
621 We determined the metabolic profile of each focal strain by measuring their ability to use 96 carbon sources
622 supplied individually in the wells of Biolog AN microplates (Endotell AG, Switzerland). Under anaerobic
623 conditions, we resuspended the carbon sources of the Biolog AN microplate in 100 µl of the manufacturer
624 inoculation fluid (AN-IF) and inoculated focal strains (original untagged version) by sampling 1 µl from
625 independent overnight cultures (incubated at 37 °C statically and anaerobically in 200 µl LB in microplates) with
626 a 96-pin microplate replicator. We sealed the microplates in an air-tight bag, which we incubated at 37 °C,
627 shaking. After 24 h, we measured OD600 in each well. We profiled metabolism of the six strains in three
628 experimental blocks and for each plate subtracted the value of the blank well from the value obtained in the
629 other wells. We considered a given substrate usable by a given strain if standard error of mean subtracted from
630 the mean was higher than the arbitrary threshold of 0.1 (Supplementary Fig. 6). We defined focal-strain nutrient
631 niche size as the number of usable substrates. We quantified average growth by each focal strain on its niche by
632 computing the mean OD600 across usable substrates. Finally, we assessed focal-strain private niche size in each
633 microbiome sample based on the binarized version of the six metabolic profiles shown on Fig. 4a: we computed
634 the number of usable substrates that a given focal strain could use that another strain (representing the most
635 abundant resident *E. coli* in each microbiome sample) could not use.
636
637 **Data availability**
638 Sequences of the 16S rRNA amplicons from the six microbiome samples and of the genome of the six *E. coli*
639 strains are uploaded to ENA (European Nucleotide Archive) and will be accessible through project PRJEB80311
640 upon publication. All other data supporting the findings of this study will be made available through an open
641 source repository upon publication.

642 # References


643 1. Dominguez-Bello MG, Costello EK, Contreras M *et al.* Delivery mode shapes the acquisition and structure of
644 the initial microbiota across multiple body habitats in newborns. *Proceedings of the National Academy of*
645 *Sciences* 2010;**107**:11971–5.

646 2. Bokulich NA, Chung J, Battaglia T *et al.* Antibiotics, birth mode, and diet shape microbiome maturation during
647 early life. *Sci Transl Med* 2016;**8**:343ra82.

648 3. Vandeputte D, De Commer L, Tito RY *et al.* Temporal variability in quantitative human gut microbiome profiles
649 and implications for clinical research. *Nat Commun* 2021;**12**:6740.

650 4. Faith JJ, Guruge JL, Charbonneau M *et al.* The Long-Term Stability of the Human Gut Microbiota. *Science*
651 2013;**341**:1237439.

652 5. Garud NR, Pollard KS. Population Genetics in the Human Microbiome. *Trends in Genetics* 2020;**36**:53–67.

653 6. Martinson JNV, Walk ST. Escherichia coli residency in the gut of healthy human adults. *EcoSal Plus*
654 2020;**9**:10.1128/ecosalplus.ESP-0003–2020.

655 7. Schloissnig S, Arumugam M, Sunagawa S *et al.* Genomic variation landscape of the human gut microbiome.
656 *Nature* 2013;**493**:45–50.

657 8. Falony G, Joossens M, Vieira-Silva S *et al.* Population-level analysis of gut microbiome variation. *Science*
658 2016;**352**:560–4.

659 9. Martínez I, Maldonado-Gomez MX, Gomes-Neto JC *et al.* Experimental evaluation of the importance of
660 colonization history in early-life gut microbiota assembly. *eLife* 2018, DOI: 10.7554/eLife.36521.

661 10. Spragge F, Bakkeren E, Jahn MT *et al.* Microbiome diversity protects against pathogens by nutrient blocking.
662 *Science* 2023;**382**:eadj3502.

663 11. Rakoff-Nahoum S, Foster KR, Comstock LE. The evolution of cooperation within the gut microbiota. *Nature*
664 2016;**533**:255–9.

665 12. Granato ET, Meiller-Legrand TA, Foster KR. The Evolution and Ecology of Bacterial Warfare. *Curr Biol*
666 2019;**29**:R521–37.

667 13. Frazão N, Konrad A, Amicone M *et al.* Two modes of evolution shape bacterial strain diversity in the
668 mammalian gut for thousands of generations. *Nat Commun* 2022;**13**:5604.

669 14. Maltby R, Leatham-Jensen MP, Gibson T *et al.* Nutritional Basis for Colonization Resistance by Human
670 Commensal Escherichia coli Strains HS and Nissle 1917 against E. coli O157:H7 in the Mouse Intestine. *PLOS ONE*
671 2013;**8**:e53957.

672 15. Marchesi JR, Ravel J. The vocabulary of microbiome research: a proposal. *Microbiome* 2015;**3**:31.

673 16. Kawecki TJ, Ebert D. Conceptual issues in local adaptation. *Ecology Letters* 2004;**7**:1225–41.

674 17. Blanquart F, Kaltz O, Nuismer SL *et al.* A practical guide to measuring local adaptation. *Ecology Letters*
675 2013;**16**:1195–205.

676 18. Leimu R, Fischer M. A Meta-Analysis of Local Adaptation in Plants. *PLOS ONE* 2008;**3**:e4010.

677 19. Hawthorne DJ, Via S. Genetic linkage of ecological specialization and reproductive isolation in pea aphids.
678 *Nature* 2001;**412**:904–7.

679 20. Marková S, Lanier HC, Escalante MA *et al.* Local adaptation and future climate vulnerability in a wild rodent.
680 *Nat Commun* 2023;**14**:7840.

681 21. Butaitė E, Kramer J, Kümmerli R. Local adaptation, geographical distance and phylogenetic relatedness:
682 Assessing the drivers of siderophore-mediated social interactions in natural bacterial communities. *Journal of*
683 *Evolutionary Biology* 2021;**34**:1266–78.

684 22. Kraemer SA, Kassen R. Patterns of local adaptation in space and time among soil bacteria. *Am Nat*
685 2015;**185**:317–31.

686 23. Scanlan PD, Hall AR, Buckling A. Parasite genetic distance and local adaptation in co-evolving bacteria–
687 bacteriophage populations. *Molecular Ecology* 2017;**26**:1747–55.

688 24. Koskella B, Thompson JN, Preston GM *et al.* Local biotic environment shapes the spatial scale of
689 bacteriophage adaptation to bacteria. *Am Nat* 2011;**177**:440–51.

690 25. Vos M, Birkett PJ, Birch E *et al.* Local Adaptation of Bacteriophages to Their Bacterial Hosts in Soil. *Science*
691 2009;**325**:833–833.

692 26. Suez J, Zmora N, Segal E *et al.* The pros, cons, and many unknowns of probiotics. *Nat Med* 2019;**25**:716–29.

693 27. Carlström CI, Field CM, Bortfeld-Miller M *et al.* Synthetic microbiota reveal priority effects and keystone
694 strains in the Arabidopsis phyllosphere. *Nat Ecol Evol* 2019;**3**:1445–54.

695 28. Brochet S, Quinn A, Mars RA *et al.* Niche partitioning facilitates coexistence of closely related honey bee gut
696 bacteria. Xavier KB, Rutz C, Xavier KB (eds.). *eLife* 2021;**10**:e68583.

697 29. Weiss AS, Burrichter AG, Durai Raj AC *et al.* In vitro interaction network of a synthetic gut bacterial
698 community. *ISME J* 2022;**16**:1095–109.

699 30. Weiss AS, Niedermeier LS, von Strempel A *et al.* Nutritional and host environments determine community
700 ecology and keystone species in a synthetic gut bacterial community. *Nat Commun* 2023;**14**:4780.

701 31. Barroso-Batista J, Sousa A, Lourenço M *et al.* The First Steps of Adaptation of Escherichia coli to the Gut Are
702 Dominated by Soft Sweeps. *PLOS Genetics* 2014;**10**:e1004182.

703 32. Nguyen TLA, Vieira-Silva S, Liston A *et al.* How informative is the mouse for human gut microbiota research?
704 *Dis Model Mech* 2015;**8**:1–16.

705 33. Baumgartner M, Bayer F, Pfrunder-Cardozo KR *et al.* Resident microbial communities inhibit growth and
706 antibiotic-resistance evolution of Escherichia coli in human gut microbiome samples. *PLOS Biology*
707 2020;**18**:e3000465.

708 34. Riley MA, Gordon DM. The ecological role of bacteriocins in bacterial competition. *Trends in Microbiology*
709 1999;**7**:129–33.

710 35. Gordon DM, O'Brien CL. Bacteriocin diversity and the frequency of multiple bacteriocin production in
711 Escherichia coli. *Microbiology* 2006;**152**:3239–44.

712 36. Wang SP, Rubio LA, Duncan SH *et al.* Pivotal Roles for pH, Lactate, and Lactate-Utilizing Bacteria in the
713 Stability of a Human Colonic Microbial Ecosystem. *mSystems* 2020;**5**:e00645-20.

714 37. Gilbert J, Blaser MJ, Caporaso JG *et al.* Current understanding of the human microbiome. *Nat Med*
715 2018;**24**:392–400.

716 38. Bäumler AJ, Sperandio V. Interactions between the microbiota and pathogenic bacteria in the gut. *Nature*
717 2016;**535**:85–93.

718 39. Fierer N, Jackson RB. The diversity and biogeography of soil bacterial communities. *Proceedings of the*
719 *National Academy of Sciences* 2006;**103**:626–31.

720 40. McCallum G, Tropini C. The gut microbiota and its biogeography. *Nat Rev Microbiol* 2024;**22**:105–18.

721 41. Cummings JH, Macfarlane GT. The control and consequences of bacterial fermentation in the human colon.
722 *J Appl Bacteriol* 1991;**70**:443–59.

723 42. Duncan SH, Louis P, Thomson JM *et al.* The role of pH in determining the species composition of the human
724 colonic microbiota. *Environmental Microbiology* 2009;**11**:2112–22.

725 43. Hove H, Mortensen PB. Influence of intestinal inflammation (IBD) and small and large bowel length on fecal
726 short-chain fatty acids and lactate. *Dig Dis Sci* 1995;**40**:1372–80.

727 44. Raulo A, Bürkner P-C, Finerty GE *et al.* Social and environmental transmission spread different sets of gut
728 microbes in wild mice. *Nat Ecol Evol* 2024;**8**:972–85.

729 45. Eberl C, Weiss AS, Jochum LM *et al. E. coli* enhance colonization resistance against *Salmonella* Typhimurium
730 by competing for galactitol, a context-dependent limiting carbon source. *Cell Host & Microbe* 2021;**29**:1680-
731 1692.e7.

732 46. Hol FJ, Voges MJ, Dekker C *et al.* Nutrient-responsive regulation determines biodiversity in a colicin-mediated
733 bacterial community. *BMC Biology* 2014;**12**:68.

734 47. Arredondo-Alonso S, Pöntinen AK, Gama JA *et al.* Plasmid-driven strategies for clone success in Escherichia
735 coli. 2024:2023.10.14.562336.

736 48. Felsenstein J. Phylogenies and the Comparative Method. *The American Naturalist* 1985;**125**:1–15.

737 49. Herlemann DP, Labrenz M, Jürgens K *et al.* Transitions in bacterial communities along the 2000 km salinity
738 gradient of the Baltic Sea. *ISME J* 2011;**5**:1571–9.

739 50. Callahan BJ, McMurdie PJ, Rosen MJ *et al.* DADA2: High resolution sample inference from Illumina amplicon
740 data. *Nat Methods* 2016;**13**:581–3.

741 51. Callahan BJ, Sankaran K, Fukuyama JA *et al.* Bioconductor Workflow for Microbiome Data Analysis: from raw
742 reads to community analyses. *F1000Res* 2016;**5**:1492.

743 52. Hong Nhung P, Ohkusu K, Mishima N *et al.* Phylogeny and species identification of the family
744 *Enterobacteriaceae* based on *dnaJ* sequences. *Diagnostic Microbiology and Infectious Disease* 2007;**58**:153–61.

745 53. Martinson JNV, Pinkham NV, Peters GW *et al.* Rethinking gut microbiome residency and the
746 Enterobacteriaceae in healthy human adults. *ISME J* 2019;**13**:2306–18.

747 54. Hu D, Fuller NR, Caterson ID *et al.* Single-gene long-read sequencing illuminates Escherichia coli strain
748 dynamics in the human intestinal microbiome. *Cell Reports* 2022;**38**:110239.

749 55. Ruppé E, Lixandru B, Cojocaru R *et al.* Relative Fecal Abundance of Extended-Spectrum-β-Lactamase-
750 Producing Escherichia coli Strains and Their Occurrence in Urinary Tract Infections in Women. *Antimicrob Agents*
751 *Chemother* 2013;**57**:4512–7.

752 56. Chang AC, Cohen SN. Construction and characterization of amplifiable multicopy DNA cloning vehicles
753 derived from the P15A cryptic miniplasmid. *Journal of Bacteriology* 1978;**134**:1141–56.

754 57. Kiss J, Szabó M, Hegyi A *et al.* Identification and Characterization of oriT and Two Mobilization Genes
755 Required for Conjugative Transfer of Salmonella Genomic Island 1. *Front Microbiol* 2019;**10**:457.

756 58. Hall BG, Acar H, Nandipati A *et al.* Growth Rates Made Easy. *Molecular Biology and Evolution* 2014;**31**:232–
757 8.

758 59. Travisano M, Lenski RE. Long-Term Experimental Evolution in Escherichia Coli. IV. Targets of Selection and
759 the Specificity of Adaptation. *Genetics* 1996;**143**:15–26.

760 60. Wick RR, Judd LM, Gorrie CL *et al.* Unicycler: Resolving bacterial genome assemblies from short and long
761 sequencing reads. *PLoS Comput Biol* 2017;**13**:e1005595.

762 61. Tian R, Zhou J, Imanian B. PlasmidHunter: accurate and fast prediction of plasmid sequences using gene
763 content profile and machine learning. *Briefings in Bioinformatics* 2024;**25**:bbae322.

764 62. Seemann T. Prokka: rapid prokaryotic genome annotation. *Bioinformatics* 2014;**30**:2068–9.

765 63. Page AJ, Cummins CA, Hunt M *et al.* Roary: rapid large-scale prokaryote pan genome analysis. *Bioinformatics*
766 2015;**31**:3691–3.

767 64. Price MN, Dehal PS, Arkin AP. FastTree 2 – Approximately Maximum-Likelihood Trees for Large Alignments.
768 *PLOS ONE* 2010;**5**:e9490.

769 65. Arndt D, Grant JR, Marcu A *et al.* PHASTER: a better, faster version of the PHAST phage search tool. *Nucleic*
770 *Acids Res* 2016;**44**:W16–21.

771 66. van Heel AJ, de Jong A, Song C *et al.* BAGEL4: a user-friendly web server to thoroughly mine RiPPs and
772 bacteriocins. *Nucleic Acids Research* 2018;**46**:W278–81.

773 67. Eberhart LJ, Deringer JR, Brayton KA *et al.* Characterization of a Novel Microcin That Kills Enterohemorrhagic
774 Escherichia coli O157:H7 and O26. *Applied and Environmental Microbiology* 2012;**78**:6592–9.

775 68. Zhao Z, Orfe LH, Liu J *et al.* Microcin PDI regulation and proteolytic cleavage are unique among known
776 microcins. *Sci Rep* 2017;**7**:42529.

777 69. Ma J, Pan Z, Huang J *et al.* The Hcp proteins fused with diverse extended-toxin domains represent a novel
778 pattern of antibacterial effectors in type VI secretion systems. *Virulence* 2017;**8**:1189–202.

779 70. Allsopp LP, Bernal P. Killing in the name of: T6SS structure and effector diversity. *Microbiology*
780 2023;**169**:001367.

781 71. Gilchrist CLM, Chooi Y-H. clinker & clustermap.js: automatic generation of gene cluster comparison figures.
782 *Bioinformatics* 2021;**37**:2473–5.

783 72. Wendling CC, Refardt D, Hall AR. Fitness benefits to bacteria of carrying prophages and prophage-encoded
784 antibiotic-resistance genes peak in different environments. *Evolution* 2021;**75**:515–28.

785

786

## Acknowledgements

We thank the Pathogen Ecology group, Carolin Wendling and Angus Buckling for their feedback.

## Funding

Funding source: Swiss National Science Foundation project 310030_192428.